

# Signals Correlation Algorithm For Cheaper Surveys: Using Windowing Functions.

M. T. Atemkeng<sup>1</sup>, O. M. Smirnov<sup>12\*</sup>, C. Tasse<sup>123</sup>, G. Foster<sup>124</sup>, J. Jonas<sup>12</sup>

<sup>1</sup>Department of Physics and Electronics, Rhodes University, PO Box 94, Grahamstown, 6140, South Africa

<sup>2</sup>SKA South Africa, 3rd Floor, The Park, Park Road, Pinelands, 7405, South Africa

<sup>3</sup>GEPI, Observatoire de Paris, CNRS, Université Paris Diderot, 5 place Jules Janssen, 92190 Meudon, France

<sup>4</sup>xxxxx

in original form 1988 October 11

## ABSTRACT

This paper investigates the use of baseline dependent windowing functions in interferometry data to minimize the loss of signal amplitude (smearing) when the correlated data is averaged over wide bandwidth and long time. In radio interferometry smearing is reduced when a cross-correlator averages the correlated data over narrower bandwidth and shorter integration times. Unfortunately, this leads to a huge amount of data to manage and it is becoming a bottleneck for further data processing such as calibration and imaging. With future generation surveys, it is important to investigate the reduction of the output data rate. Therefore, the focus of this paper is on the use of baselines dependent windowing functions to keep smearing down at an acceptable extent and at the same time significantly suppress signals from out field of view sources, while the nominal sensitivity is conserved.

**Key words:** Instrumentation: interferometers, Methods: data analysis, Methods: numerical, Techniques: interferometric

## 1 INTRODUCTION

The recent radio astronomy techniques is to build a single, gigantic instrument called *interferometer*, from the combination of several small parabolic antennas separated over kilometres (?). The signal from each antenna is combined at the level of a cross-correlator to form the interferometer data output. The cross-correlator carries out data reduction and filters out an amount of noise by averaging the signal of each baseline over discrete time and/or frequency bins. It is well known in interferometry that averaging can lead to the loss of signal amplitude when the cross correlator integrate over a longer period of time and a wider bandwidth. This effect is known as time-average smearing and bandwidth smearing (Thompson *et al.* ?). The above effects cause the distortion of sources within the field of interest by decreasing their intensity.

To keep smearing down at acceptable levels, a correlator must cross-correlate the signal over a shorter period of time and a narrower bandwidth, hence producing a large amount of data for subsequence stage such as imaging (Martí-Vidal & Marcaide 2008; Linfield 1986), calibration (?), etc. This

huge amount of data is becoming an increasingly serious problem and becoming more challenging as the computational demands of the next generation radio telescopes will rise significantly (see the SKA phase 1 specification ?). Similarly, the next generation of radio telescopes will require an unprecedented level of SNR while mapping large regions of the sky. Thus, a substantial increase in SNR can only be achieve by observing for longer time at wider bandwidth without loss of signal: this is not realisable with averaging. Therefore, it becomes urgent to develop new decorrelation algorithm techniques that will allow the required SNR of the future radio telescopes.

In this paper, we investigate the efficiency of correlator windowing functions for the reduction of interferometric data and the recovery of interferometers arrays desire FoV, with the ultimate goal of reaching higher SNR. The main idea is to achieve a high SNR by conserving the astrophysical signal and by limiting the noise. Thermal noise can be driven arbitrary low by increasing the observing time<sup>1</sup>, but in radio astronomy confusion noise is a major problem and can even cause calibration to fail. Therefore, we seek to use a windowing function that will conserve the useful signal while

\* E-mail: o.smirnov@ru.ac.za (OMS); m.atemkeng@gmail.com (MTA); cyril.tasse@obspm.fr (CT); griffin.foster@gmail.com (GF); j.jonas@ru.ac.za (JJ)

also limiting sidelobes confusion from out of FoV sources.

$$\text{SNR} = \frac{S_{\text{use}}}{N_{\text{ter}} + N_{\text{con}}} \quad (1)$$

- "Useful signal",  $S_{\text{use}}$  the signal from source in the field of interest. These sources should be accurately recovered over the instrument entire FoV : correlator windowing functions maximized this signal by allowing the interferometer array to map a large region of the sky.

- "Sidelobe confusion",  $N_{\text{con}}$  signal from out field of view sources received from their sidelobes. These sources are not of interest and should be removed : correlator windowing functions acts as a remover of these signals when the array is mapping a large region of the sky.

- "Thermal noise",  $N_{\text{ter}}$  the thermal noise from the instrument, ionosphere, etc. Averaging presents theoretically a maximum sensitivity, but the use of extended correlator windowing functions can reduce or eliminate the loss of the nominal sensitivity.

The proposed techniques are applied to MeerKAT (Karoo Array Telescope) ? and the Very Large Array (VLA)? and could also be used for future radio telescopes such as the SKA.

## 2 OVERVIEWS AND DEFINITIONS

### 2.1 Visibility and relation with the sky

An interferometer array measured a quantity  $V = V(u, v, w)$  known classically as the visibility function (see ?). The variables  $u, v$  and  $w$  are in unit of wavelength and they are the coordinates of the vector of which the norm is the distance between two antennas, known in interferometry as a baseline. A source in the sky will see  $u$  and  $v$  oriented towards the direction East-West and South-North respectively and  $w$  is directed towards the phase centre of the source plane or image plane. The projection of  $u$  and  $v$  in the image plane are  $l$  and  $m$  respectively. They are the observed source coordinates, measured in radian. The ideal measurement of interferometric wide-field imaging also known as the van Cittert-Zernike theorem (Thompson et al. 2001, Eq.6) is given by

$$V_{pq} = \int \int \frac{I(l, m)}{\sqrt{1 - l^2 - m^2}} e^{-2\pi i \phi(u, v, w)} dl dm, \quad (2)$$

where  $I(l, m)$  is the sky brightness and  $\phi(u, v, w) = u.l + v.m + w.(\sqrt{1 - l^2 - m^2} - 1)$  is a term from the cross-correlator that models the direction in the sky and the separation of the two antennas. The term  $\sqrt{1 - l^2 - m^2}$  is the result of the projection of the celestial sphere on the image plane.

### 2.2 Averaging and convolution

The Earth rotation causes the phase,  $\phi(u, v, w)$  to variate in time. The baseline coordinates are defined in units of wavelength, and making  $\phi(u, v, w)$  to variate in frequency. To take this effect into account, Eq. 2 is rewritten as an integration over time and frequency interval. If we consider that  $[t_s, t_e]$

is the time integration interval and  $[\nu_s, \nu_e]$  the frequency integration interval, then Eq.2 can be rewritten as:

$$V_{pq}^{\text{avg}} = \frac{1}{\Delta t \Delta \nu} \int_{t_s}^{t_e} \int_{\nu_s}^{\nu_e} V_{pq}(t, \nu) d\nu dt \quad (3)$$

$V_{pq}$  is a continuous function, in reality we know only the sampled visibility,  $V_{pq,(t,\nu)}^{\text{samp}} = S_{pq,(t,\nu)} V_{pq,(t,\nu)}$  at a specific time and frequency.  $S_{pq,(t,\nu)}$  is a sampling function that indicates where the  $(u, v)$  data for the baseline  $(p, q)$  is measured during the time and frequency integration. Therefore, Eq.3 holds for many sources, when the signal at the centre frequency,  $\nu_c$  and at the centre time,  $t_c$  is restricted to a narrow frequency interval and to a short time interval  $[t_s, t_e]$  respectively, this is the current efficient observing mode. However, this is expressed mathematically as

$$V_{pq}^{\text{avg}} = \frac{1}{n_t n_\nu} \sum_{i=1}^{n_t} \sum_{j=1}^{n_\nu} S_{pq,(t_i, \nu_j)} V_{pq,(t_i, \nu_j)}. \quad (4)$$

Here,  $n_t$  and  $n_\nu$  are the number of discrete times within the time interval and the number of discrete frequency within the frequency interval respectively. For convenience, lets introduce a normalized *Boxcar* windowing function,  $\Pi_{pq,(t_c - t_i, \nu_c - \nu_j)}$  that will attribute an equal weight (in this case  $1/n_t n_\nu$ ) to all sampling visibilities points. We can therefore rewrite Eq. 4 as:

$$V_{pq}^{\text{avg}} = \sum_{i=1}^{n_t} \sum_{j=1}^{n_\nu} \Pi_{pq,(t_c - t_i, \nu_c - \nu_j)} S_{pq,(t_i, \nu_j)} V_{pq,(t_i, \nu_j)} \quad (5)$$

$$= \sum_{i=1}^{n_t} \sum_{j=1}^{n_\nu} \Pi_{pq,(t_c - t_i, \nu_c - \nu_j)} V_{pq,(t_i, \nu_j)}^{\text{samp}}. \quad (6)$$

It is worth noting that Eq.6 is a naturally weighted visibility and is a two dimensional convolution between the *Boxcar* windowing function and the sampled visibility  $V_{pq}^{\text{samp}}$ . Thus, averaging is equivalent to convolving the sampled visibility with a *Boxcar* windowing function. Mathematically, this is described as follows:

$$V_{pq}^{\text{avg}} = c_{pq,(t,\nu)} \cdot \left( \left( \Pi_{pq} \circ V_{pq}^{\text{samp}} \right)_{(t,\nu)} \right). \quad (7)$$

Here,  $c_{pq,(t,\nu)}$  is a function that samples the result of  $\left( \Pi_{pq} \circ V_{pq}^{\text{samp}} \right)_{(t,\nu)}$  at the centre time interval and centre frequency interval.

### 2.3 Effect of time and bandwidth averaging

During imaging, Eq.7 is inverse Fourier transform, and after applying the convolution theorem, the *sinc* function ( $\mathcal{F}^{-1} \Pi_{pq,(t,\nu)} = \text{sinc}(\pi \Delta u_{pq} ||1||)$ ) multiply the sky. Thus, the sky map is tapered by the *sinc* function in the  $l$  and  $m$  direction, the response is maximal for sources at the phase centre ( $l = 0, m = 0$ ) while for off-phase centre sources, the response is smeared (decreased) for larger  $\Delta u_{pq}$  ( $\Delta u_{pq}$  is a function of  $\Delta t$  and  $\Delta \nu$ ). The main lobe of the *sinc* extends from  $-1/2\Delta u_{pq}$  to  $1/2\Delta u_{pq}$  while the amplitude gradually dies out, and the larger the  $\Delta u_{pq}$ , the narrower the central peak and the oscillations. Therefore, the degree of smear-

ing increases with the position of a source and the baseline length (see Thompson et al.)<sup>2</sup>.

(i) Fig.1 shows the attenuation of a source at various coordinates in the sky for various integration time interval. We measure more than 90% of the source brightness for integrations less than or equal to 25s when the source is within the Field of view and more than 90% when the source is out of the Field of View. As mention above, for small integration like 25s we produce large data and maintain strong sidelobes contamination from out field of view sources.

(ii) Fig.3

Fortunately, since the response is maximal only for sources at the phase centre, an interesting approach is achieved by convolving the observed visibility with a windowing function that depends on  $(u, v)$  coordinates spacing (baseline dependent windowing function). However, a windowing function with a wide dynamic range spectrum is preferable in this work.

## 2.4 Imaging

From the full sky Radio Interferometry Measurement Equation (RIME) formalism (see Hamaka et al, O.M. Smirnov (2010a)), in this case, the sampled visibilities can be presented mathematically as a  $4 \times n_t \times n_v$  matrix of four polarizations time and frequency dependent matrices each of size  $n_t \times n_v$ .

$$\begin{aligned} \mathbf{V}_{pq,(t,v)}^{samp} &= \mathbf{S}_{pq,(t,v)} \cdot \mathbf{V}_{pq,(t,v)} \\ &= \left( \mathbf{V}_{pq,(t,v)}^0, \mathbf{V}_{pq,(t,v)}^1, \mathbf{V}_{pq,(t,v)}^2, \mathbf{V}_{pq,(t,v)}^3 \right)^T. \end{aligned}$$

Now, consider that  $\mathbf{W}_{pq,(t,v)}$  is a  $n_t \times n_v$  matrix that contained the weights of the baseline  $(p, q)$  visibilities points. The weights of this matrix are given by a baseline dependent windowing function that we described in section 3 and section 4. The convolution operator is linear, therefore we can rewrite Eq.7 in terms of a series of linear transformations as follow:

$$\mathbf{V}_{pq}^{avg} = \mathbf{W}_{pq,(t,v)}^{block} \cdot \mathbf{S}_{pq,(t,v)} \cdot \mathbf{V}_{pq,(t,v)}. \quad (8)$$

Here,  $\mathbf{W}_{pq,(t,v)}^{block}$  is a block diagonal matrix of size  $(4n_t n_v) \times (4n_t n_v)$  and the block elements are  $\mathbf{C}_{pq,(t,v)} \cdot \mathbf{W}_{pq,(t,v)}$  of size  $n_t \times n_v$ , where  $\mathbf{C}_{pq,(t,v)}$  is the centre time interval and centre frequency interval sampling matrix of size  $n_t \times n_v$ . This is the result of the time and frequency integration for the baseline  $(p, q)$ .

For a synthesis, the baseline  $(p, q)$  made a full coverage in the  $(u, v)$  plane. Therefore, we can package into a single matrix,  $\mathbf{V}_{pq}^{avg}$  of size  $(4N_t N_v) \times (4N_t N_v)$  the weighted average visibilities of the baseline  $(p, q)$  during the synthesis as follows:

$$\mathbf{V}_{pq}^{avg} = \mathbf{W}_{pq,(t,v)}^{block,n} \cdot \mathbf{S}_{pq,(t,v)}^n \cdot \mathbf{V}_{pq,(t,v)}, \quad (9)$$

<sup>2</sup> The Fourier phase components  $2\pi\phi(u, v, w)$  depends on the direction in the sky, the wavelength, the separation of antennas as well as the integration time and frequency. A maximal phase will occurs on longer baselines and small phase on shorter baselines.

where  $N_t$  and  $N_v$  are the number of time sample and frequency channels entering the Fourier domain. If the synthesis time is  $T$  and the frequency range is  $F$ , then  $T = N_t \times \Delta t$  and  $F = N_v \times \Delta\nu$ . The the size of  $\mathbf{V}_{pq}^{avg}$  can also be written as  $(4N_v^{pq}) \times (4N_v^{pq})$ , where  $N_v^{pq}$  is the number of time and frequency visibilities for the baseline  $(p, q)$ . The matrix  $\mathbf{W}_{pq,(t,v)}^{block,n}$  is a diagonal block matrix of size  $(4N_v^{pq} n_t n_v) \times (4N_v^{pq} n_t n_v)$  where each diagonal block is the block diagonal matrix  $\mathbf{W}_{pq,(t,v)}^{block}$  defined above and  $n$  is the number of  $\mathbf{W}_{pq,(t,v)}^{block}$ . The sampled visibilities  $\mathbf{S}_{pq,(t,v)}^n \cdot \mathbf{V}_{pq,(t,v)} = \mathbf{V}_{pq,(t,v)}^{smp,n}$  is a one row matrix of size  $(N_v^{pq} 4n_t n_v) \times (4n_t n_v)$  made of  $\mathbf{V}_{pq,(t,v)}^{smp}$  on top of each other.

$$\mathbf{V}_{pq}^{avg} = \mathbf{W}_{pq,(t,v)}^{block,n} \cdot \mathbf{S}_{pq,(t,v)}^n \cdot \mathbf{F} \cdot \mathcal{I}_{l,m}^{sky}, \quad (10)$$

if the number of pixel in the sky model is  $N_{pix}$ , then the true sky image vector  $\mathcal{I}_{l,m}^{sky}$  has a size of  $4N_{pix}$  and  $\mathbf{F}$  is the Fourier transform operator of size  $(4N_{pix}) \times (4N_{pix})$ .

We are generally interested in using the total set of visibilities over baselines, time and frequencies, having  $4 \times N_v$  visibilities measured over all baselines and  $N_v = n_{bl} \times N_v^{pq}$  in this case. Here,  $n_{bl}$  is the number of baseline. We can write

$$\mathbf{V}_{all}^{avg} = \mathbf{A} \cdot \mathcal{I}_{l,m}^{sky}. \quad (11)$$

Here,  $\mathbf{A}$  is a matrix of size  $(4N_v) \times (4N_{pix})$  made of  $\mathbf{W}_{pq,(t,v)}^{block,n} \cdot \mathbf{S}_{pq,(t,v)}^n \cdot \mathbf{F}$  on top of each other. The dirty image,  $\mathcal{I}_{l,m}^D$  of size  $4N_{pix}$  can then be derived

$$\mathcal{I}_{l,m}^D = \mathbf{F}^H \cdot \mathbf{A} \cdot \mathcal{I}_{l,m}^{sky}. \quad (12)$$

Here,  $H$  represents the the conjugate transpose operation also known as a Hermitian transpose and  $\mathbf{F}^H$  is the inverse Fourier transform operator of size  $(4N_{pix}) \times (4N_{pix})$ .

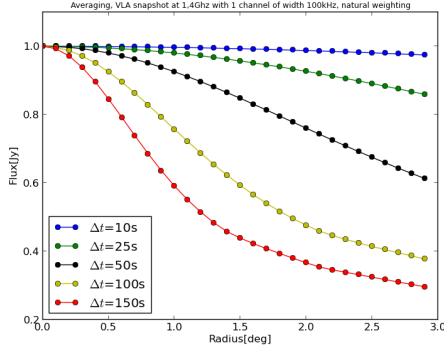
## 3 DATA COMPRESSION ALGORITHM

### 3.1 Description

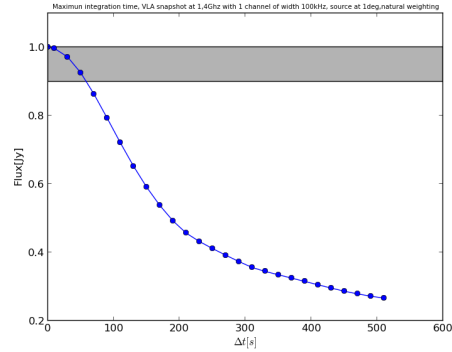
Missing spaces between sampled  $(u, v)$  coordinates has huge dependences on the baseline length. However, the spacing between longer baselines  $(u, v)$  coordinates are wider then the one on shorter baselines: this explained while sources are more distorted on longer baselines. We aims in this section, to describe the algorithm we use with a baseline-dependent windowing function to assign a proper weight to a data reference by a  $(u, v)$  coordinate considering the *spacing*<sup>3</sup> between the baseline  $(u, v)$  coordinates.

Fig.5 shows a snapshot coverage of an integration interval. For shorter baselines, the tracks are closer to the centre of rotation and for longer baselines the tracks are farther away from this centre. The *dot marks* are the data for a sampled  $(u, v)$  data, and the arrows indicates the separation between  $(u, v)$  coordinates and the centre  $(u, v)$  coordinate. It is trivial to see on this figure that these separations are wider

<sup>3</sup> The *distance* has also huge dependences on the baseline length and allow us to formally define the data weight of a  $uv$  point over the entire  $uv$  plane.



**Figure 1.** The fall of the intensity of a 1Jy source move from the phase centre for  $\Delta t$  integration synthesis at 100KHz bandwidth.



**Figure 2.** (b) Response to a 1Jy source at 1deg, as a function of  $\Delta t$  with 100KHz bandwidth

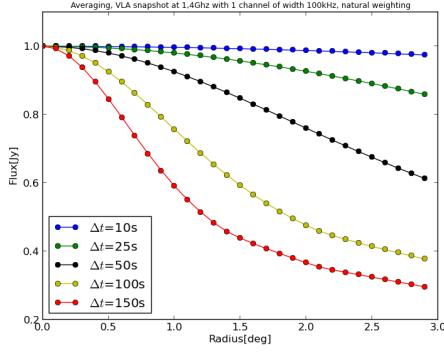


**Figure 3.** The fall of the intensity of a 1Jy source move from the phase centre for  $\Delta t$  integration synthesis at 100KHz bandwidth.

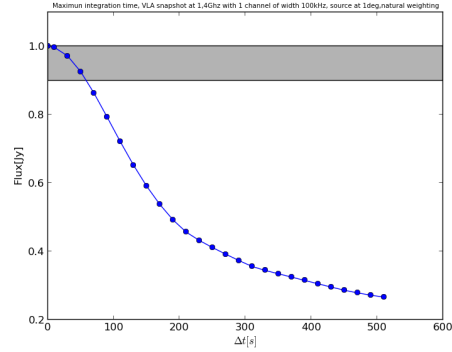


**Figure 4.** The fall of the intensity of a 1Jy source move from the phase centre for  $\Delta t$  integration synthesis at 100KHz bandwidth.

on longer baselines. The results of averaging is assigned to the centre  $(u, v)$  coordinate coloured in red.

### 3.2 Methods

In this section, we present the data compression algorithm we use to describe the weight of each sampled visibility during the integration time interval and frequency interval. Now, let package the  $(u, v)$  coordinates changes of a baseline  $pq$  into a single matrix of size  $n_t \times 2$ .

$$\mathbf{U}_{pq,t} = \begin{pmatrix} \mathbf{u}_{pq,t_s}, \dots, \mathbf{u}_{pq,t_c}, \dots, \mathbf{u}_{pq,t_e} \end{pmatrix}^T, \quad (13)$$

where the indexes  $s$ ,  $c$  and  $e$  references the integration interval starting, centre, and ending time respectively. The elements of  $\mathbf{U}_{pq,t}$  are functions of time and frequency representing a  $(u, v)$  coordinate. The frequency changes of the baseline coordinates can be package into a single vector of dimension  $n_v$

$$\mathbf{v} = \begin{pmatrix} v_s, \dots, v_c, \dots, v_e \end{pmatrix}^T$$

We define a norm,  $\|\cdot\|_m$  on a  $n_t \times 2$  matrix as follow:

$$\|\mathbf{U}_{pq,t}\|_m = \left( \|\mathbf{u}_{pq,t_s}\|, \dots, \|\mathbf{u}_{pq,t_c}\|, \dots, \|\mathbf{u}_{pq,t_e}\| \right), \quad (14)$$

where  $\|\cdot\|$  is the Euclidean norm.

**Definition 1.1. (Time direction spacing)** The matrix that model the spacing between the  $(u, v)$  coordinates and the centre  $(u, v)$  coordinate of a baseline  $(p, q)$  across the time direction is defined as

$$\mathbf{U}_{pq,t}^s = \frac{v_c}{c} \cdot \left\{ \mathbf{U}_{pq,t} - \mathbf{H}_{pq,t} \right\},$$

where  $c$  is the speed of the light and  $\mathbf{H}_{pq}$  is a matrix of size  $n_t \times 2$  that model the centre  $uv$ -coordinate,  $\mathbf{H}_{pq,t} = (\mathbf{u}_{pq,t_s}, \dots, \mathbf{u}_{pq,t_c}, \dots, \mathbf{u}_{pq,t_e})^T$ .

**Definition 1.2. (Frequency direction spacing)** The vector of size  $n_v$  that model the spacing between the  $(u, v)$  coordinates and the centre  $(u, v)$  coordinate of a baseline  $(p, q)$  across the frequency direction is defined as

$$\mathbf{d}_v^T = \frac{\|\mathbf{u}_{pq,t_c}\|}{c} \cdot \left\{ \mathbf{v} - v_c \cdot \mathbf{g}_v^T \right\},$$

where  $\mathbf{g}$  is a  $1 \times n_v$  unity matrix.

**Definition 1.3. (Baseline dependent windowing function)**

If  $f_{pq}$  is a baseline dependent windowing function, then:

$$f_{pq} : \{\mathcal{R}, \mathcal{R}\} \rightarrow \mathcal{R}$$

$$d_{t_i}, d_{v_j} \mapsto \frac{w_{t_i, v_j}}{\sum_{i=1}^{n_t} \sum_{j=1}^{n_v} w_{t_i, v_j}}.$$

where  $d_{t_i}$  is an element of the vector  $\mathbf{d}_t = \|\mathbf{U}_{pq,t}^s\|_m$  and  $d_{v_j}$  is an element of the vector  $\mathbf{d}_v^T$ .

**3.3 Noise analysis**

For convenience, in this section, we analyse the centre pixel noise of a sky map after we had apply a baseline dependent windowing function during the time and frequency integration. The brightness of the naturally weighted central pixel is estimate by (see the inverse Fourier transform of equation (19-2) in ? ).

$$\begin{aligned} \tilde{\mathcal{I}}(0,0) &= \frac{1}{N_v} \sum_{k=1}^{N_v} V_{all,k}^{avg} \\ &= \frac{1}{N_v} \sum_{pq,k=1}^{N_v^{pq}} V_{pq,k}^{avg} \\ &= \frac{1}{N_v} \sum_{pq,k=1}^{N_v^{pq}} \left( \sum_{i=1}^{n_t} \sum_{j=1}^{n_v} f_{pq,(d_{t_i}, d_{v_j})} V_{pq,(t_i, v_j)}^{samp} \right). \end{aligned}$$

Here, the variable  $k$  run through the baseline  $(p, q)$  timeslots. The overall rms noise is given by

$$\sigma^2 = \frac{\sigma_{samp}^2}{N_v^2} \left( \sum_{pq,k=1}^{N_v^{pq}} \sum_{i=1}^{n_t} \sum_{j=1}^{n_v} f_{pq,(d_{t_i}, d_{v_j})}^2 \right),$$

where  $\sigma_{samp}$  is the per sampled visibility noise

**4 OUT FOV SOURCES SUPPRESSION ALGORITHM****4.1 Description**

In theory, windowing functions and signals generally extend to infinity. Unfortunately, in practice, filtering a signal with a low pass filter, one need to define a cut-off interval. Therefore, if one wants to achieve sufficiently an accurate estimate of the windowing function ideal spectrum, one need a wide cut-off interval as far as the spectrum approaches the ideal when the windowing function order increases. An overlap baseline dependent windowing function aims to extend the order of the baseline dependent windowing function in such a way that, we approaches the ideal spectrum. The only drawback of this technique is the increased of the time needed for processing the output sample of the signals being integrate.

**4.2 Methods**

The weight of a visibility is not defined by a unique baseline dependent windowing, but by the strength of the correlation between the overall overlapping baseline dependent windowing functions on the visibility. Now, consider that  $f_{pq}^a$  is an overlap-BDWF of width  $\Delta t$  and  $\Delta v$  across the time and frequency direction respectively.

**Definition 1.4. (Baseline dependent windowing function)**

if  $\Delta_t t$  and  $\Delta_t v$  are the overlap time interval and frequency interval of the baseline dependent windowing function  $f_{pq}^{a_0}$  respectively and  $\{f_{pq}^{a_1}, f_{pq}^{a_2}, f_{pq}^{a_3}, \dots\}$  the set of BDWF overlapping on the left hand side of  $f_{pq}^{a_0}$  then the resulting BDWF within  $\Delta_t t$  and  $\Delta_t v$  is defined as

$$g_{pq}^{lhs} : \{\mathcal{R}, \mathcal{R}\} \rightarrow \mathcal{R}$$

$$d_{t_i}, d_{v_j} \mapsto \frac{1}{N_{lhs}} \left( \sum_k f_{pq,(d_{t_i}, d_{v_j})}^{a_k} + f_{pq,(d_{t_i}, d_{v_j})}^{a_0} \right).$$

Here,  $N_{lhs}$  is the normalization term defined as

$$N_{lhs} = \sum_{i=1}^{n_{lt}} \sum_{j=1}^{n_{lv}} \left( \sum_k f_{pq,(d_{t_i}, d_{v_j})}^{a_k} + f_{pq,(d_{t_i}, d_{v_j})}^{a_0} \right),$$

where  $n_{lt}$  and  $n_{lv}$  are the number of  $(u, v)$  coordinates changes and frequency changes within  $\Delta_t t$  and  $\Delta_t v$  respectively.

**Definition 1.5. (Baseline dependent windowing function)**

if  $\Delta_r t$  and  $\Delta_r v$  are the overlap time and frequency interval of a BDWF  $f_{pq}^{a_0}$  respectively and  $\{f_{pq}^{a_1}, f_{pq}^{a_2}, f_{pq}^{a_3}, \dots\}$  the set of BDWF overlapping on the right hand side of  $f_{pq}^{a_0}$ , then the resulting BDWF within  $\Delta_r t$  and  $\Delta_r v$  is defined as

$$g_{pq}^{rhs} : \{\mathcal{R}, \mathcal{R}\} \rightarrow \mathcal{R}$$

$$d_{t_i}, d_{v_j} \mapsto \frac{1}{N_{rhs}} \left( f_{pq,(d_{t_i}, d_{v_j})}^{a_0} + \sum_k f_{pq,(d_{t_i}, d_{v_j})}^{a_k} \right).$$

Here,  $N_{rhs}$  is the normalization term defined as

$$N_{rhs} = \sum_{i=1}^{n_{rt}} \sum_{j=1}^{n_{rv}} \left( f_{pq,(d_{t_i}, d_{v_j})}^{a_0} + \sum_k f_{pq,(d_{t_i}, d_{v_j})}^{a_k} \right),$$

where  $n_{rt}$  and  $n_{rv}$  are the number of  $(u, v)$  coordinates changes and frequency changes within  $\Delta_r t$  and  $\Delta_r v$  respectively.

From the above definitions, the following derivation is trivial

$$\{\Delta_t, \Delta_v\} = \{\Delta_t t \cup \Delta_u t \cup \Delta_r t, \Delta_t v \cup \Delta_u v \cup \Delta_r v\},$$

where  $\Delta_u t$  and  $\Delta_u v$  are  $f_{pq}^{a_0}$  uncorrelated time and frequency interval respectively. They follows the below rules

$$\Delta_u t = \begin{cases} \cup \{t_i\}_{i=s', s' \geq s+1}^{c', c' \leq c-1} & \text{if } n_{lt} + n_{rt} < n_t \\ \{t_c\} & \text{if } n_{lt} + n_{rt} = n_t \\ \emptyset & \text{otherwise} \end{cases}$$

$$\Delta_u v = \begin{cases} \cup \{v_i\}_{i=s', s' \geq s+1}^{c', c' \leq c-1} & \text{if } n_{lv} + n_{rv} < n_v \\ \{v_c\} & \text{if } n_{lv} + n_{rv} = n_v \\ \emptyset & \text{otherwise} \end{cases}$$

The resulting BDWF becomes  $g_{pq}$  described as

$$g_{pq} = \begin{cases} g_{pq}^{lhs} & \text{if } (t, v) \in (\Delta_t t, \Delta_t v) \\ f_{pq}^{a_0} & \text{if } (t, v) \in (\Delta_u t, \Delta_u v) \\ g_{pq}^{rhs} & \text{if } (t, v) \in (\Delta_r t, \Delta_r v) \end{cases}$$

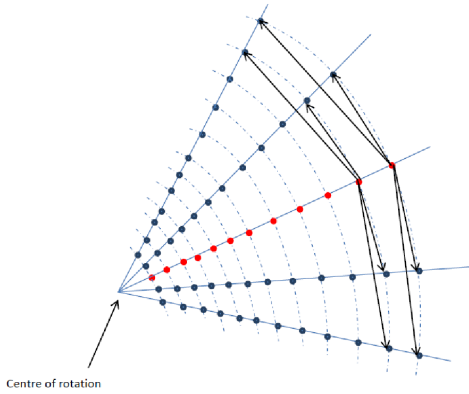


Figure 5. Snapshot coverage

### 4.3 Noise analysis

The overall rms noise is given by

$$\sigma^2 = \frac{\sigma_{smp}^2}{N_v^2} \left( \sum_{pq,k=1}^{N_0^{pq}} \sum_{i=1}^{n_t} \sum_{j=1}^{n_v} \delta_{pq,(dt_i,dv_j)}^2 \right),$$

### 4.4 Windowing functions

In signal processing a windowing function is a mathematical function that is zero-values outside of some chosen interval, and when another function or a signal is multiplied by the windowing function, the product is also zero-values outside the interval. In this section, we evaluation the Peak Sidelobe Level (PSL), the Main Lobe width (MLW) and the Sidelobes Roll-off (SLR) of some windowing functions spectrum. This study will allow us to make a suitable choice of the window that by tapering with the sky, we conserve the brightness of sources in the field of interest and attenuate sidelobes confusion from strong sources out of the field of interest.

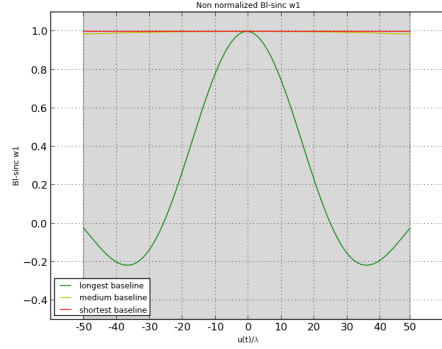
#### 4.4.1 Boxcar window: natural weighting

This windowing function take a hunk of the data without modification, and this leads to discontinuities at the edges<sup>4</sup>. For a cut-off frequency interval  $[-\nu_a, \nu_a]$  the boxcar windowing function is defined as:

$$\Pi_u = \begin{cases} 1 & -\nu_a \leq \nu \leq \nu_a \\ 0 & \text{otherwise} \end{cases} \quad (15)$$

Fig.7 and Fig.8 gives the graph of  $\Pi_u$  and its spectrum respectively. The blue and the red curve of Fig.8 are the spectrum of  $\Pi_u$  for a frequency cut-off interval,  $[-\nu_a, \nu_a]$  and  $[-\nu_a/2, \nu_a/2]$  respectively. We noticed that when the cut-off interval is large, the MLW of the spectrum is narrower, the PSL is lower and the SLR drop faster.

<sup>4</sup> unless it happens that the signal fit exactly with the windowing function width. Nevertheless, it is rare to find such a situation.

Figure 6.  $Bl-sincw1$  used to convolve the visibility data obtained from the long, medium and short baseline

#### 4.4.2 Gaussian window

A Gaussian windowing function centred at mean zero with standard deviation,  $\sigma$  can be described as

$$G_u = e^{-bv^2}. \quad (16)$$

Here,  $b = (2\sigma^2)^{-1}$  and  $\mathcal{F}^{-1}\{G_u\} = \sqrt{\frac{b}{\pi}} e^{-c l^2}$ , where  $c = \pi^2/b$ . This shows us that the inverse Fourier transform of a Gaussian with standard deviation  $\sigma$  is a Gaussian with a standard deviation  $\sigma' = (2\pi\sigma)^{-1}$ .

Fig.13 and Fig.14 gives the graph of  $G_u$  and its spectrum respectively, where  $G_u$  is truncate within the cut-off frequency interval  $[-\nu_a, \nu_a]$ , with  $b = 3$  for the blue curve and  $b = 5$  for the red one. We noticed that when the standard deviation is large, the MLW of the spectrum is narrower, the PSL is higher and the SLR drop slowly compare to a smaller standard deviation.

#### 4.4.3 Butterworth

The frequency response of the Butterworth filter is flat in the pass band, and rolls off towards zero in the stop band, and it is characterized by two independent parameters, the cut-off frequency  $\nu_a$  and the order  $p$ . These two parameters controls the bandwidth and side lobes attenuation. The frequency response of the Butterworth is given by

$$B_u = \left(1 + (\nu/\nu_a)^{2p}\right)^{-1}. \quad (17)$$

For the same frequency interval  $[-\nu_a, \nu_a]$ , we plotted three curves  $\{p = 1, p = 3, p = 5\}$  of  $B_u$  in Fig.11 and their corresponding spectrum in Fig.12. We noticed that when the other  $p$  is getting bigger, the MLW of the spectrum is conserved, while the PSL is getting higher and the SLR is dropping faster.

#### 4.4.4 Bessel Function of the First Kind

#### 4.4.5 First order prolate spheroidal wave function

#### 4.4.6 Sinc window

In theory, the sinc window is an infinitely large convolution filter as it is non zero everywhere, and its inverse Fourier

Transform produces the ideal filter kernel (the boxcar windowing function). The sinc is defined as follow:

$$S_u = \text{sinc}(\pi b u(t/\lambda_a)). \quad (18)$$

However, in practice some one need to defined a cut-off interval where the window is considered to be non zero, and zero out of this cut-off interval. Fig.9 and Fig.10 gives the graph of  $S_u$  and its spectrum respectively, where  $S_u$  is truncate within the cut-off frequency interval  $[-\nu_a, \nu_a]$ . We noticed that when the cut-off frequency interval is large (Fig.10, blue curve), the spectrum becomes perfectly flat at the pass-band while the MLW becomes narrower, the PSL becomes lower and the SLR drop faster compare to a cut-off frequency of  $[-\nu_a, \nu_a]$  (Fig.10, red curve).

Windows	MLL (-3db)	PSL (db)	SLR (db/octave)
$\Pi_u$	$\approx 0,073$	-6,68	-6,78
$\mathcal{F}^{-1}\{\Pi_u\}$	$\approx 0,306$	-11,22	-12,42
$G_u$	$\approx 0,0736$	-30,28	-14,5
$B_u$	$\approx 0,079$	-10,08	-15,39
$P_u$	$\approx -$	-	-

A windowing function with a narrower main lobe width for a better spectral resolution, lower PSL to have less masking of nearby sources, and faster SLR to have less masking for far away sources is preferably in this work. Nevertheless, The energy is more concentrated in the frequency domain main lobe when the lobe width is narrower. Therefore, the frequency domain of the boxcar and the Butterworth window look similar, but the other of the Butterworth frequency domain can be control with the goal to concentrate more energy in the frequency main lobe. However, the sinc window is preferable as we expect in this work, signals in a wide dynamic range.

#### 4.4.7 Noise and comparison

The methods described in section (3) and section (4) are use in this subsection to evaluate the theoretical noise,  $f_{pq}$  and  $g_{pq}$  are replaced in Eq.15 and Eq.15 respectively by the windowing functions described above. Table (4.4.7) and (4.4.7) summarize the theoretical noise where these functions are used as a baseline dependent windowing and as an overlap baseline dependent windowing functions respectively.

$f_{pq}$	Theoretical noise	$g_{pq}$	Theoretical noise
$\Pi_u$	1,066	$\Pi_u$	1,066
$\mathcal{F}^{-1}\{\Pi_u\}$	1,066	$\mathcal{F}^{-1}\{\Pi_u\}$	1,066
$G_u$	1,334	$G_u$	1,334
$B_u$	1,066	$B_u$	1,066
$\mathcal{F}^{-1}\{B_u\}$	1,066	$\mathcal{F}^{-1}\{B_u\}$	1,066
$P_u$	1,334	$P_u$	1,334

1.) In Figure 1.) In Figures (??) and (??) we represented the ratio  $\frac{\sigma_{meas,pq}}{\sigma_{av,pq}}$  as a function of  $\sum_i^n u_i((t_c - t_i)/\lambda)$  ( $\sigma_{meas,pq}, \sigma_{av,pq}$  are the per baselines CWF and averaging rms noise respectively). We could also represented it as a function of baseline length. But, a uv-track corresponding

to baseline aligned along the Est-West direction has longer tracts compare to one aligned along the South-Nordth for the same integration and frequency band. Therefore,  $\frac{\sigma_{meas,pq}}{\sigma_{av,pq}}$  v/s baselines length is ambiguous. We consider five baselines dependent windowing sinc function, *Bl-sinc wk* (with an extended width of  $(k-1)n$  time intervals and/or frequency channels and  $k \geq 1$ ). The experiment is done for two cases, figure (??) is the one for *Bl-sinc wk* over both time-frequency and figure (??) over time. These figures shows that, the noise increases with baselines length.

2.) Figure (??) shows that, with *Bl-sinc wk*, the noise is lower on shorter baselines compared to the longer baselines. This is because on shorter baselines  $\frac{\sigma_{meas,pq}}{\sigma_{av,pq}} \approx \frac{n}{n+k}$ , it is the same case with Figure (??) where  $\frac{\sigma_{meas,pq}}{\sigma_{av,pq}} \approx \sqrt{\frac{n}{n+k}}$  (see the proof). With *Bl-Sinc wk* ( $k > 1$ ), the noise drops with the extended number of time intervals and/or frequency channels of the window. The rate of this drop is non-linear with baselines length and also with the overlap time interval and/or frequency channels (see figure (??b) and (??b), the variation of the noise rate between baselines).

3.) In spite of the overlapping, with the theoretical results, the noise of longer baselines do not drop when the overlap samples is increased (figure ??). The reason is, few windows are overlapping in a visibility point when we extended in a unique direction (the time interval in this case) compare to two directions (time interval and frequency channels). The theoretical derivation for the overall noise of *Bl-sinc wk* and the simulated one are quantified similarly but the pattern of the per baseline simulated rms noise do not look the same with the theoretical one. The number of  $k$  determines the amount of noise of CWF.

## 5 SIMULATION AND RESULTS

In order to test the algorithms described in section and section, we performed multiple tests on JVLA simulated measurement set (dataset). In this section we summarize and discussed those results. In order to test the two algorithms we described above, we used a JVLA simulated high resolution dataset of 11min15s synthesis, with a 1,5s integration time at 1.4Ghz, with 150 channels of width 125Khz. From the high resolution dataset, we apply the methods and saved the results to a low resolution dataset, of 1min30s synthesis, with a 150s integration time at 1.4Ghz, with 1 channels of width 6.25Mhz. In order to apply the second algorithm, we met the following conditions:

(i) A high resolution dataset has to start before the low resolution one and the number of timeslots within these two starting times has to be greater than or equal to the number of overlap timeslots.

(ii) A low resolution dataset has to end before the high resolution one and the number of timeslots within these two ending times has to be greater than or equal to the number of overlap timeslots.

The above conditions are also applied to the starting and the ending frequency channel of the two dataset. For our simulation, we took  $start\_time\_hres = 0s$  for the high resolu-

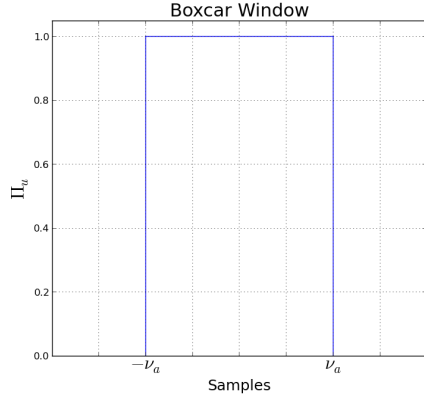


Figure 7. Boxcar windowing function.

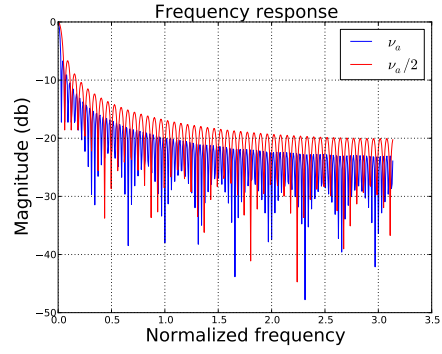


Figure 8. Overlap BDWF's:  $\Delta_u t = [225, 250]$ .

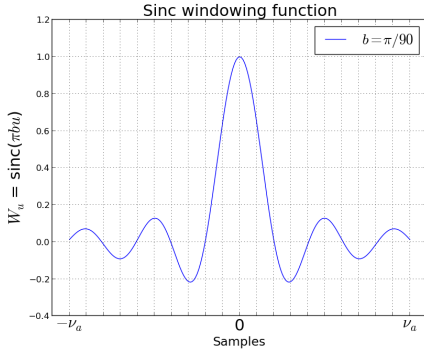


Figure 9. Overlap BDWF's:  $\Delta_u t = \{250\}$ .

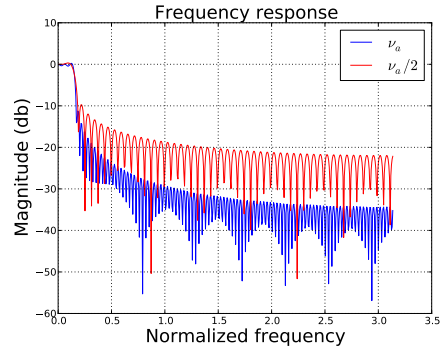


Figure 10. Overlap BDWF's:  $\Delta_u t = \emptyset$ .

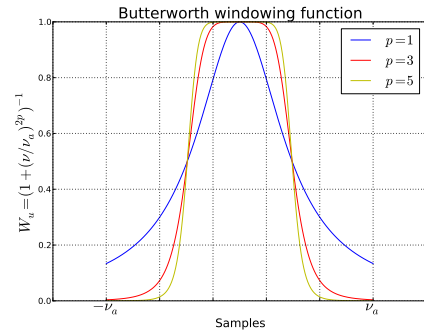


Figure 11. Overlap BDWF's:  $\Delta_u t = \{250\}$ .

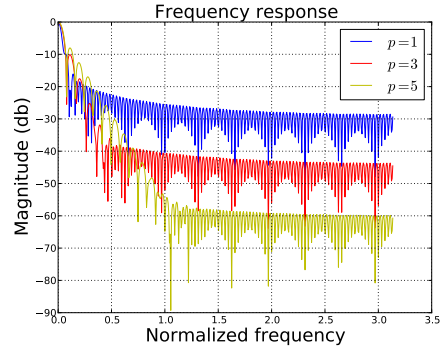


Figure 12. Overlap BDWF's:  $\Delta_u t = \emptyset$ .

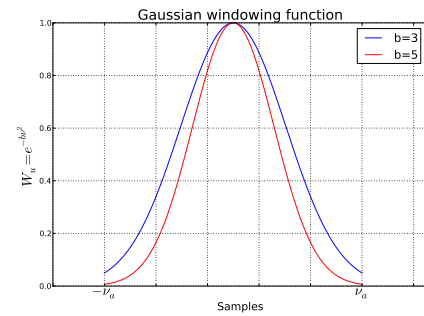


Figure 13. Overlap BDWF's:  $\Delta_u t = \{250\}$ .

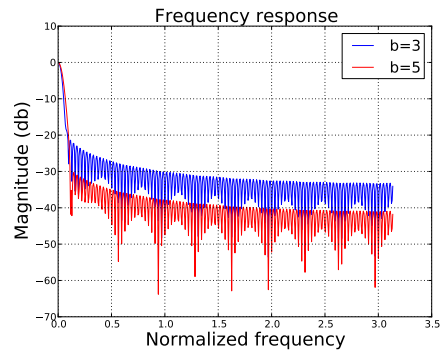
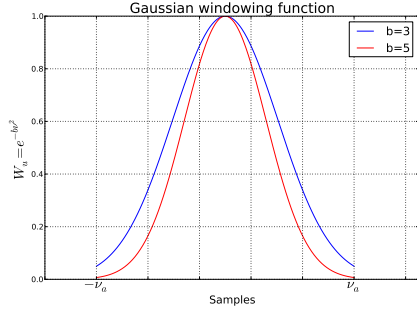
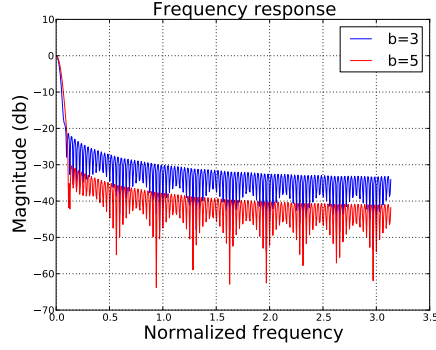
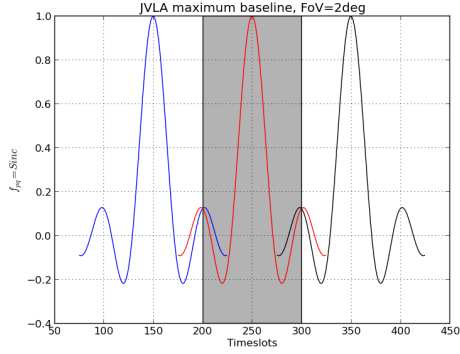
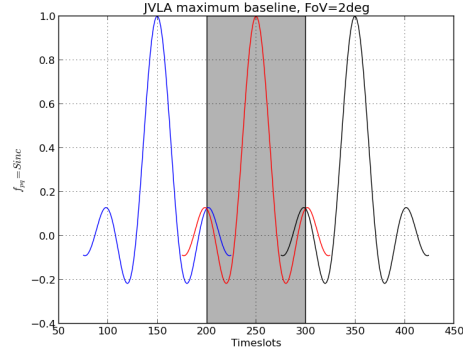
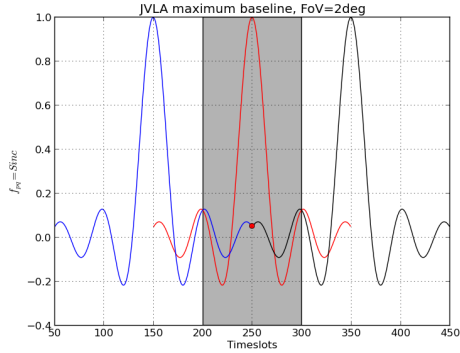
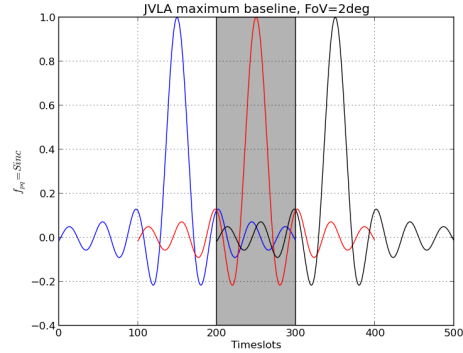


Figure 14. Overlap BDWF's:  $\Delta_u t = \emptyset$ .

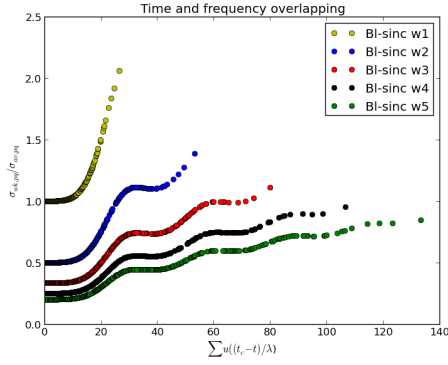


Figure 15. Overlap BDWF's:  $\Delta_u t = \{250\}$ .Figure 16. Overlap BDWF's:  $\Delta_u t = \emptyset$ .Figure 17. Overlap BDWF's:  $\Delta_u t = [225, 250]$ .Figure 18. Overlap BDWF's:  $\Delta_u t = [225, 250]$ .Figure 19. Overlap BDWF's:  $\Delta_u t = \{250\}$ .Figure 20. Overlap BDWF's:  $\Delta_u t = \emptyset$ .

tion dataset starting time, and  $start\_time\_lres = 1min30s$  for the low resolution dataset starting time. Similarly, we took  $start\_freq\_hres = 125Khz$  for the high resolution dataset starting frequency, and  $start\_freq\_lres = 6.25Mhz$  for the low resolution dataset starting frequency. We used a sinc windowing function and the Bessel function of the First Kind as a baseline dependent windowing function.

**Notations:** *Avg*: averaging,  $Bl-sinc\ Wo_t \times o_v$  and  $Bl-J_0\ Wo_t \times o_v$  are the baseline-dependent *sinc* and the Bessel function of the First Kind respectively with an extended width of  $(o_t - 1)n_t$  time bins and  $(o_v - 1)n_v$  frequency bins ( $o_t \geq 1$  and  $o_v \geq 1$ ).  $\mathcal{R}_\sigma = \frac{\sigma_w}{\sigma_{Avg}}$ : the noise ratio, with  $\sigma_w$  the resulting noise for the baseline dependent windowing function and  $\sigma_{Avg}$  the average resulting noise,  $r$ :

source position in degrees. Fig.23 and Fig.24 shows the measured brightness of a simulate 1Jy source move from the phase centre to a given position in the sky using a sinc windowing function with FoV equal to two degrees and FoV equal to four degrees respectively. We recovered about 75% of the source brightness within the FoV using  $Bl-sinc-w1 \times 1$  with 150s integration time interval and 6.25Mhz integration frequency interval and suppressed the source like averaging when this source is out FoV. This result shows that smearing is eliminated within the FoV when we are integrating over large time and frequency. The drawback is the thermal noise increases. We furthermore extends the width of the  $Bl-sinc-w1 \times 1$  window, by and amount of 100 times bins and 25 frequencies bins (see  $Bl-sinc-w100 \times 25$ ), and 150 times



**Figure 21.** Noise ratio and rate of *Bl-sinc-wk*: time in interval and frequency channels.

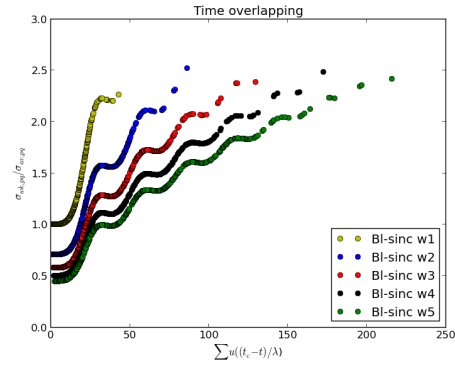


**Figure 22.** Noise ratio and rate of *Bl-sinc-wk*: time in interval.

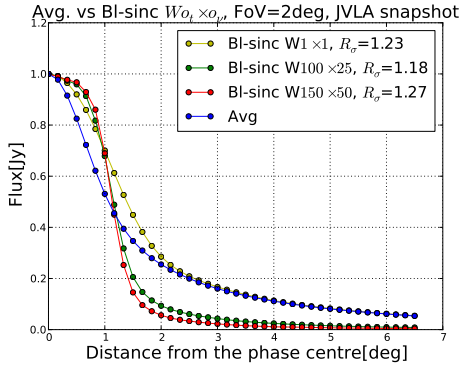


**Figure 23.** Overlap BDWF's:  $\Delta_u t = [225, 250]$ .

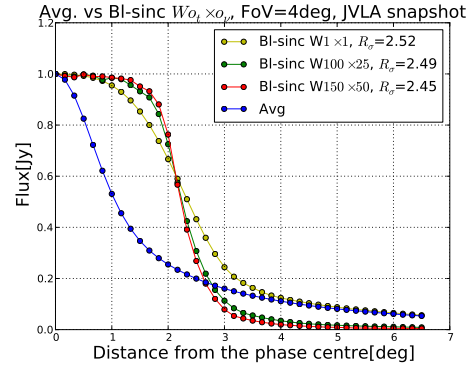


**Figure 24.** Overlap BDWF's:  $\Delta_u t = [225, 250]$ .

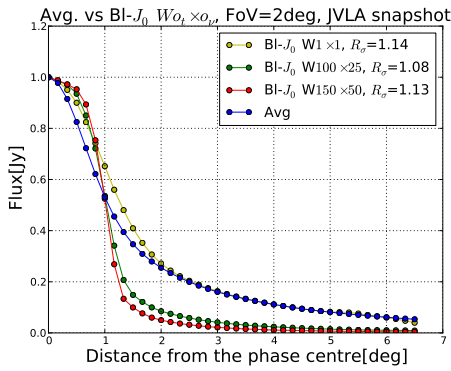


**Figure 25.** Overlap BDWF's:  $\Delta_u t = \{250\}$ .

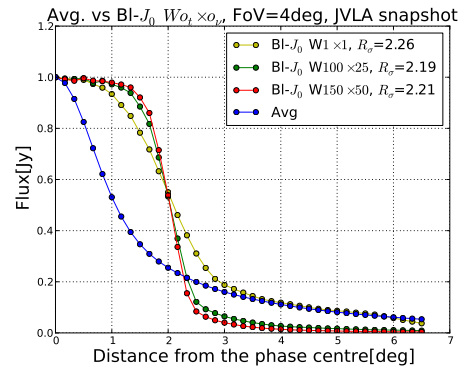


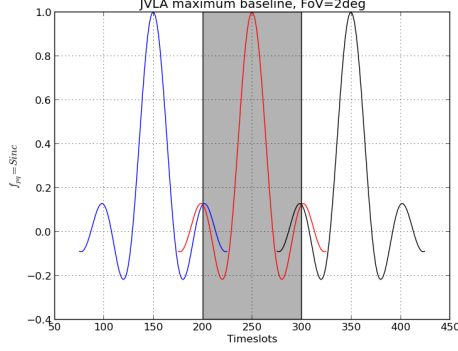
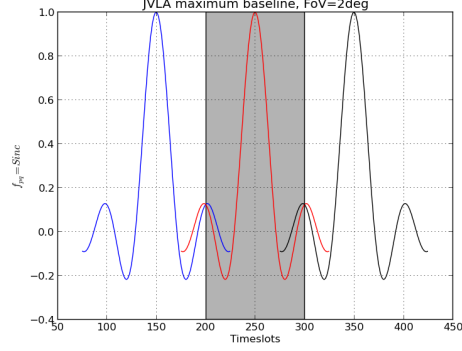
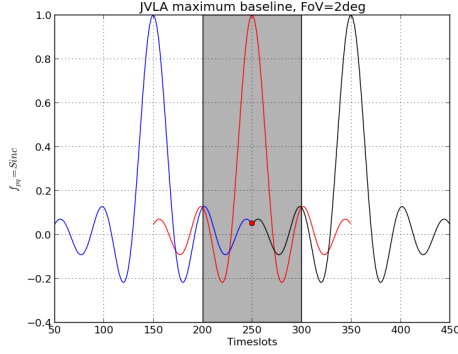
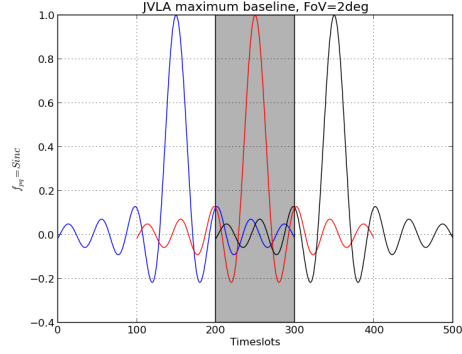
**Figure 26.** Overlap BDWF's:  $\Delta_u t = \emptyset$ .

bins and 50 frequencies bins (see *Bl-sinc-w150*  $\times$  50). We noticed that, by doing this, we recovered more brightness of the source and we more suppressed the source when this is out of the FoV, this by conserving or reducing the same amount of thermal noise given by the *Bl-sinc-w1*  $\times$  1 window. From these Figures, we could conclude that, when the extend width grows up, we recover more brightness within the FoV and suppressed more out of this FoV.

## 5.1 Discussion

## 6 CONCLUSIONS

The goal of this paper was threefold. The first objective was to investigate \*\*\*\* windowing functions\*\*\*  
The second objective was to study \*\*\*\*first algorithm data compression\*\*\*  
The final objective was to \*\*\*\*second algorithm data compression and out field suppression\*\*\*  
Drawback and futures works\*\*\* drawback and futures works\*\*\*\*

Figure 27. Overlap BDWF's:  $\Delta_{it} = [225, 250]$ .Figure 28. Overlap BDWF's:  $\Delta_{it} = [225, 250]$ .Figure 29. Overlap BDWF's:  $\Delta_{it} = \{250\}$ .Figure 30. Overlap BDWF's:  $\Delta_{it} = \emptyset$ .

## ACKNOWLEDGEMENTS

## REFERENCES

- Linfield R., 1986, AJ, 92, 213  
 Martí-Vidal I., Marcaide J., 2008, A&A, 480, 289  
 Perlis S., 1952, Theory of matrices. Dover Publications

## APPENDIX A: DEMONSTRATION

The proof of the norm used in Section 3.2 is given below.

if  $\|\mathbf{U}_{pq,t}\|_m = \left( \|\mathbf{u}_{pq,t_s}\|, \dots, \|\mathbf{u}_{pq,t_c}\|, \dots, \|\mathbf{u}_{pq,t_e}\| \right)$  is a  $n_t \times 2$  matrix, where each element  $\mathbf{u}_{pq,t_i}$  is a vector of size 2 and  $\|\cdot\|$  is an Euclidean norm, then  $\|\cdot\|_m$  is a norm.

*Proof.* (i) For all  $\mathbf{u}_{pq,t_k}$ ,  $\|\mathbf{u}_{pq,t_k}\| \geq 0$ . Therefore, all the elements of the vector  $\|\mathbf{U}_{pq,t}\|_m$  are positives.

(ii) Let  $\mathbf{U}_{pq,t}$  and  $\mathbf{U}'_{pq,t}$  be two matrices with norm of

$$\|\mathbf{U}_{pq,t}\|_m = \left( \|\mathbf{u}_{pq,t_s}\|, \dots, \|\mathbf{u}_{pq,t_c}\|, \dots, \|\mathbf{u}_{pq,t_e}\| \right) \text{ and}$$

$$\text{norm of } \|\mathbf{U}'_{pq,t}\|_m = \left( \|\mathbf{u}'_{pq,t_s}\|, \dots, \|\mathbf{u}'_{pq,t_c}\|, \dots, \|\mathbf{u}'_{pq,t_e}\| \right).$$

$$\|\mathbf{U}_{pq,t} + \mathbf{U}'_{pq,t}\|_m = \left( \|\mathbf{u}_{pq,t_s} + \mathbf{u}'_{pq,t_s}\|, \dots, \|\mathbf{u}_{pq,t_c} + \mathbf{u}'_{pq,t_c}\|, \dots, \|\mathbf{u}_{pq,t_e} + \mathbf{u}'_{pq,t_e}\| \right). \text{ For all } k, \|\mathbf{u}_{pq,t_k} + \mathbf{u}'_{pq,t_k}\| \leq$$

$\|\mathbf{u}_{pq,t_k}\| + \|\mathbf{u}'_{pq,t_k}\|$ , this is trivial because  $\|\cdot\|$  is the Euclidean norm. Therefore,  $\|\mathbf{U}_{pq,t} + \mathbf{U}'_{pq,t}\|_m \leq \|\mathbf{U}_{pq,t}\|_m + \|\mathbf{U}'_{pq,t}\|_m$   
 $\square$

## APPENDIX B: DERIVATION OF COMPLEX MATRICES

The matrix  $\mathbf{W}_{pq,(t,v)}$  is of size  $n_t \times n_v$  and contained the weights of the baseline  $(p,q)$  visibilities points. The convolution operator is linear, therefore we can rewrite Eq.7 in terms of a series of linear transformations as follow:

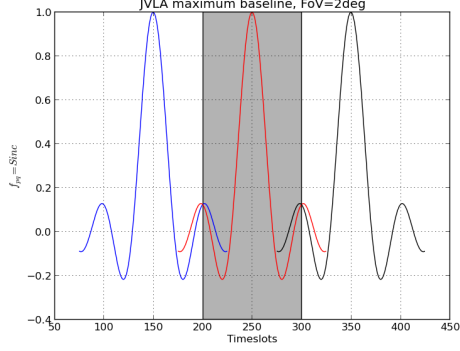
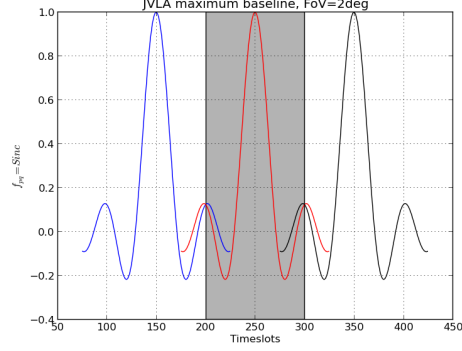
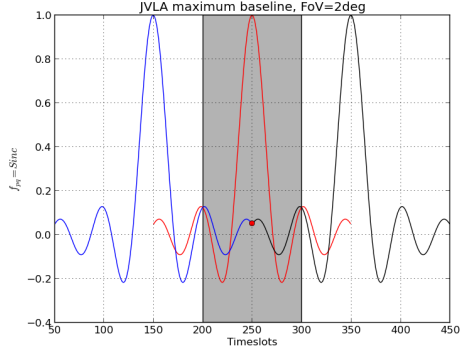
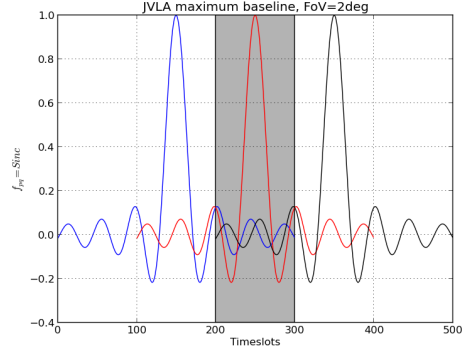
$$\mathbf{V}_{pq}^{corr} = \mathbf{C}_{(t,v)}^{block} \cdot \mathbf{W}_{pq,(t,v)}^{block} \cdot \mathbf{V}_{pq,(t,v)}^{smp}. \quad (\text{B1})$$

Here,  $\mathbf{W}_{pq,(t,v)}^{block}$  is a block diagonal matrix of size  $(4n_t n_v) \times (4n_t n_v)$  defined as follow:

$$\mathbf{C}_{(t,v)}^{block} = \begin{bmatrix} \mathbf{c}_{(t,v)} & 0 & 0 & 0 \\ 0 & \mathbf{c}_{(t,v)} & 0 & 0 \\ 0 & 0 & \mathbf{c}_{(t,v)} & 0 \\ 0 & 0 & 0 & \mathbf{c}_{(t,v)} \end{bmatrix}$$

Here,  $\mathbf{W}_{pq,(t,v)}^{block}$  is a block diagonal matrix of size  $(4n_t n_v) \times (4n_t n_v)$  defined as follow:

$$\mathbf{W}_{pq,(t,v)}^{block} = \begin{bmatrix} \mathbf{W}_{pq,(t,v)} & 0 & 0 & 0 \\ 0 & \mathbf{W}_{pq,(t,v)} & 0 & 0 \\ 0 & 0 & \mathbf{W}_{pq,(t,v)} & 0 \\ 0 & 0 & 0 & \mathbf{W}_{pq,(t,v)} \end{bmatrix}$$

Figure 31. Overlap BDWF's:  $\Delta_u t = [225, 250]$ .Figure 32. Overlap BDWF's:  $\Delta_u t = [225, 250]$ .Figure 33. Overlap BDWF's:  $\Delta_u t = \{250\}$ .Figure 34. Overlap BDWF's:  $\Delta_u t = \emptyset$ .

$$\mathbf{V}_{pq,(t,v)}^{smp} = \left[ \mathcal{V}_{pq,(t,v)}^0, \mathcal{V}_{pq,(t,v)}^1, \mathcal{V}_{pq,(t,v)}^2, \mathcal{V}_{pq,(t,v)}^3 \right]^T.$$

For a synthesis, the baseline  $(p, q)$  made a full coverage in the  $(u, v)$  plane. Therefore, we can package into a single matrix,  $\mathbf{V}_{pq}^{avg}$  of size  $(4N_t N_v) \times (4N_t N_v)$  the weighted average visibilities of the baseline  $(p, q)$  during the synthesis as follows:

$$\mathbf{V}_{pq}^{corr} = \mathbf{C}_{(t,v)}^{block,n} \cdot \mathbf{W}_{pq,(t,v)}^{block,n} \cdot \mathbf{V}_{pq,(t,v)}^{smp,n}. \quad (\text{B2})$$

where  $N_t$  and  $N_v$  are the number of time sample and frequency channels entering the Fourier domain. If the synthesis time is  $T$  and the frequency range is  $F$ , then  $T = N_t \times \Delta t$  and  $F = N_v \times \Delta \nu$ . The size of  $\mathbf{V}_{pq}^{avg}$  can also be written as  $(4N_v^{pq}) \times (4N_v^{pq})$ , where  $N_v^{pq}$  is the number of time and frequency visibilities for the baseline  $(p, q)$ . The matrix  $\mathbf{W}_{pq,(t,v)}^{block,n}$  is a diagonal block matrix of size  $(4N_v^{pq} n_t n_v) \times (4N_v^{pq} n_t n_v)$  defined as follow:

$$\mathbf{W}_{pq,(t,v)}^{block,n} = \begin{bmatrix} \mathbf{W}_{pq,(t,v)}^{block} & \dots & 0 & \dots & 0 \\ \vdots & \vdots & \vdots & \vdots & \vdots \\ 0 & \dots & \mathbf{W}_{pq,(t,v)}^{block} & \dots & 0 \\ \vdots & \vdots & \vdots & \vdots & \vdots \\ 0 & \dots & 0 & \dots & \mathbf{W}_{pq,(t,v)}^{block} \end{bmatrix}$$

$$\mathbf{C}_{(t,v)}^{block,n} = \begin{bmatrix} \mathbf{C}_{(t,v)}^{block} & \dots & 0 & \dots & 0 \\ \vdots & \vdots & \vdots & \vdots & \vdots \\ 0 & \dots & \mathbf{C}_{(t,v)}^{block} & \dots & 0 \\ \vdots & \vdots & \vdots & \vdots & \vdots \\ 0 & \dots & 0 & \dots & \mathbf{C}_{(t,v)}^{block} \end{bmatrix}$$

The sampled visibilities  $\mathbf{V}_{pq,(t,v)}^{smp,n}$  is a one row matrix of size  $(N_v^{pq} 4n_t n_v) \times (4n_t n_v)$  made of  $\mathbf{V}_{pq,(t,v)}^{smp}$  on top of each other.

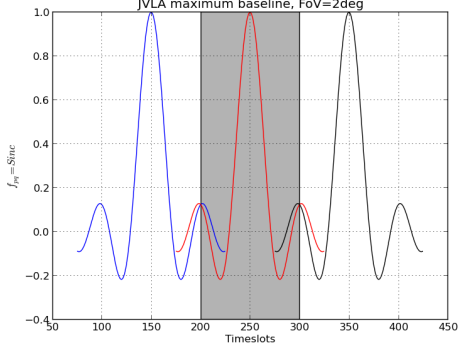
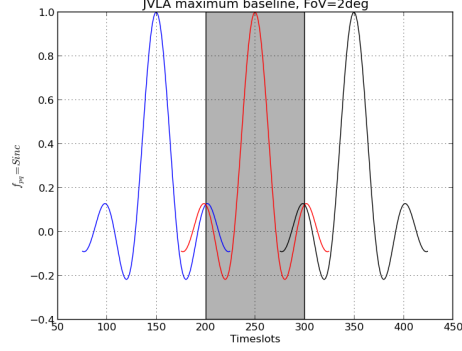
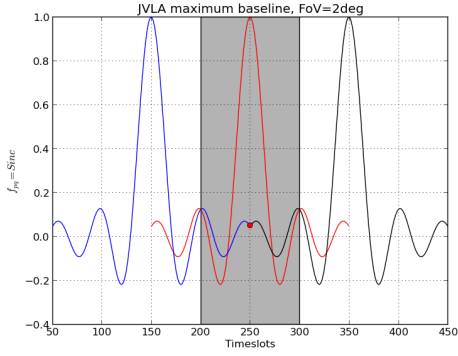
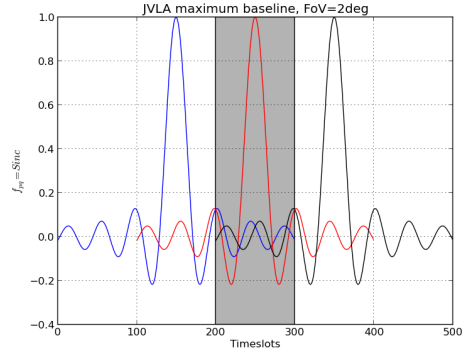
$$\mathbf{V}_{pq,(t,v)}^{smp,n} = \left[ \mathbf{V}_{pq,(t,v)}^{smp}, \dots, \mathbf{V}_{pq,(t,v)}^{smp}, \dots, \mathbf{V}_{pq,(t,v)}^{smp} \right]^T.$$

$$\mathbf{V}_{pq}^{avg} = \mathbf{W}_{pq,(t,v)}^{block,n} \cdot \mathbf{S}_{pq,(t,v)}^n \cdot \mathbf{F} \cdot \mathcal{I}_{l,m}^{sky}, \quad (\text{B3})$$

if the number of pixel in the sky model is  $N_{pix}$ , then the true sky image vector  $\mathcal{I}_{l,m}^{sky}$  has a size of  $4N_{pix}$  and  $\mathbf{F}$  is the Fourier transform operator of size  $(4N_{pix}) \times (4N_{pix})$ .

We are generally interested in using the total set of visibilities over baselines, time and frequencies, having  $4 \times N_v$  visibilities measured over all baselines and  $N_v = n_{bl} \times N_v^{pq}$  in this case. Here,  $n_{bl}$  is the number of baseline. We can write

$$\mathbf{V}_{all}^{avg} = \mathbf{A} \cdot \mathcal{I}_{l,m}^{sky}. \quad (\text{B4})$$


 Figure 35. Overlap BDWF's:  $\Delta_u t = [225, 250]$ .

 Figure 36. Overlap BDWF's:  $\Delta_u t = [225, 250]$ .

 Figure 37. Overlap BDWF's:  $\Delta_u t = \{250\}$ .

 Figure 38. Overlap BDWF's:  $\Delta_u t = \emptyset$ .

Here,  $\mathbf{A}$  is a matrix of size  $(4N_v) \times (4N_{pix})$  defined as follow

$$\mathbf{A}_{l,m} = \begin{bmatrix} \mathbf{C}_{(t,v)}^{block,n} \cdot \mathbf{W}_{01,(t,v)}^{block,n} \cdot \mathbf{S}_{01,(t,v)}^{block,n} \cdot \mathbf{F} \\ \vdots \\ \mathbf{C}_{(t,v)}^{block,n} \cdot \mathbf{W}_{ik,(t,v)}^{block,n} \cdot \mathbf{S}_{ik,(t,v)}^{block,n} \cdot \mathbf{F} \\ \vdots \\ \mathbf{C}_{(t,v)}^{block,n} \cdot \mathbf{W}_{jl,(t,v)}^{block,n} \cdot \mathbf{S}_{jl,(t,v)}^{block,n} \cdot \mathbf{F} \end{bmatrix}$$

The dirty image,  $\mathcal{I}_{l,m}^D$  of size  $4N_{pix}$  can then be derived

$$\mathcal{I}_{l,m}^D = \mathbf{F}^H \cdot \mathbf{A} \cdot \mathcal{I}_{l,m}^{sky}. \quad (\text{B5})$$

Here,  $H$  represents the the conjugate transpose operation also known as a Hermitian transpose and  $\mathbf{F}^H$  is the inverse Fourier transform operator of size  $(4N_{pix}) \times (4N_{pix})$ .

### APPENDIX C: SIMILAR WAY OF IMAGING

We explained how we derived the complex matrices used in section 2.4 Each baseline has his own baseline dependent windowing functions during integration. Unfortunately, we can not accurately estimate the resulting spectrum of all windowing functions that multiply the sky seen by these baselines (if we supposed that all baselines are seen the same sky). The measured sky intensity of the array is derived from the inverse Fourier transform of the sum of the sample visibilities measured at each baseline. The mathematics behind

this is as follow:

$$\mathcal{I}_{l,m}^D = \mathcal{F}^{-1} \left\{ \sum_{pq} \mathcal{S}_{pq} \cdot \left( c_{pq} \cdot (\mathcal{W}_{pq} \circ \mathcal{V}) \right) \right\}_{(t,v)}$$

where  $\mathcal{S}_{pq}$  is the sampling function of the baseline  $pq$ . This can be rewritten as

$$\mathcal{I}_{l,m}^D = \sum_{pq} \mathcal{B}_{pq} \circ \left( \mathcal{F}^{-1} \{c\}_{pq} \circ (\mathcal{R}_{pq} \cdot \mathcal{I}^{sky}) \right)_{(l,m)}$$

Here,  $\mathcal{R}_{pq} = \mathcal{W}_{pq}$  is the sky response or smearing response for the baseline  $pq$ . The same sky seen by all baselines is  $\mathcal{I}^{sky}$  and  $\mathcal{B}_{pq}$  is the synthesized beam or point spread function of

the baseline  $pq$ .  $\left( \mathcal{F}^{-1} \{c\}_{pq} \circ (\mathcal{R}_{pq} \cdot \mathcal{I}^{sky}) \right)_{(l,m)} = (\mathcal{R}_{pq} \cdot \mathcal{I}^{sky})_{(l,m)}$ . Therefore, the dirty beam can be written as:

$$\mathcal{I}_{l,m}^D = \left( \sum_{pq} \mathcal{B}_{pq} \circ (\mathcal{R}_{pq} \cdot \mathcal{I}) \right)_{(l,m)}$$

If the integration windowing function were the same in all baseline, then we can write:

$$\mathcal{I}_{l,m}^D = \left( \left( \sum_{pq} \mathcal{B}_{pq} \right) \circ (\mathcal{R} \cdot \mathcal{I}) \right)_{(l,m)}$$

This paper has been typeset from a  $\text{\TeX}/\text{\LaTeX}$  file prepared by the author.